Supporting Information

Enhanced Thermoelectric Performance of p-type Mg_2Sn Single Crystals via Multi-scale Defect Engineering

Zhicheng Huang,[a] Kei Hayashi,[*a] Wataru Saito,[a] Jun Pei,[b] Jing-Feng Li,[ab] Yuzuru Miyazaki [a]

[a] Department of Applied Physics, Graduate School of Engineering, Tohoku University, Sendai 980-8579, Japan

[b] State Key Laboratory of New Ceramics and Fine Processing, School of Materials Science and Engineering, Tsinghua University, Beijing, 100084, China

***Corresponding author.** E-mail address: kei.hayashi.b5@tohoku.ac.jp (K. Hayashi)

SEM observation

Figure S1a shows sample positions in the $Mg_{2-x}Li_xSn$ ingots used for each measurement. SEM images of the x = 0.02 ingot revealed that there were white dots in the edge area, whereas such dot was not found in the center area (Figures S1b and S1c, respectively). From the EDX analysis (Figure S1b1), the white dots were identified to be Sn secondary phase. The absence of the Sn secondary phase was confirmed by the elemental mapping images shown in Figures S1c1 and S1c2.

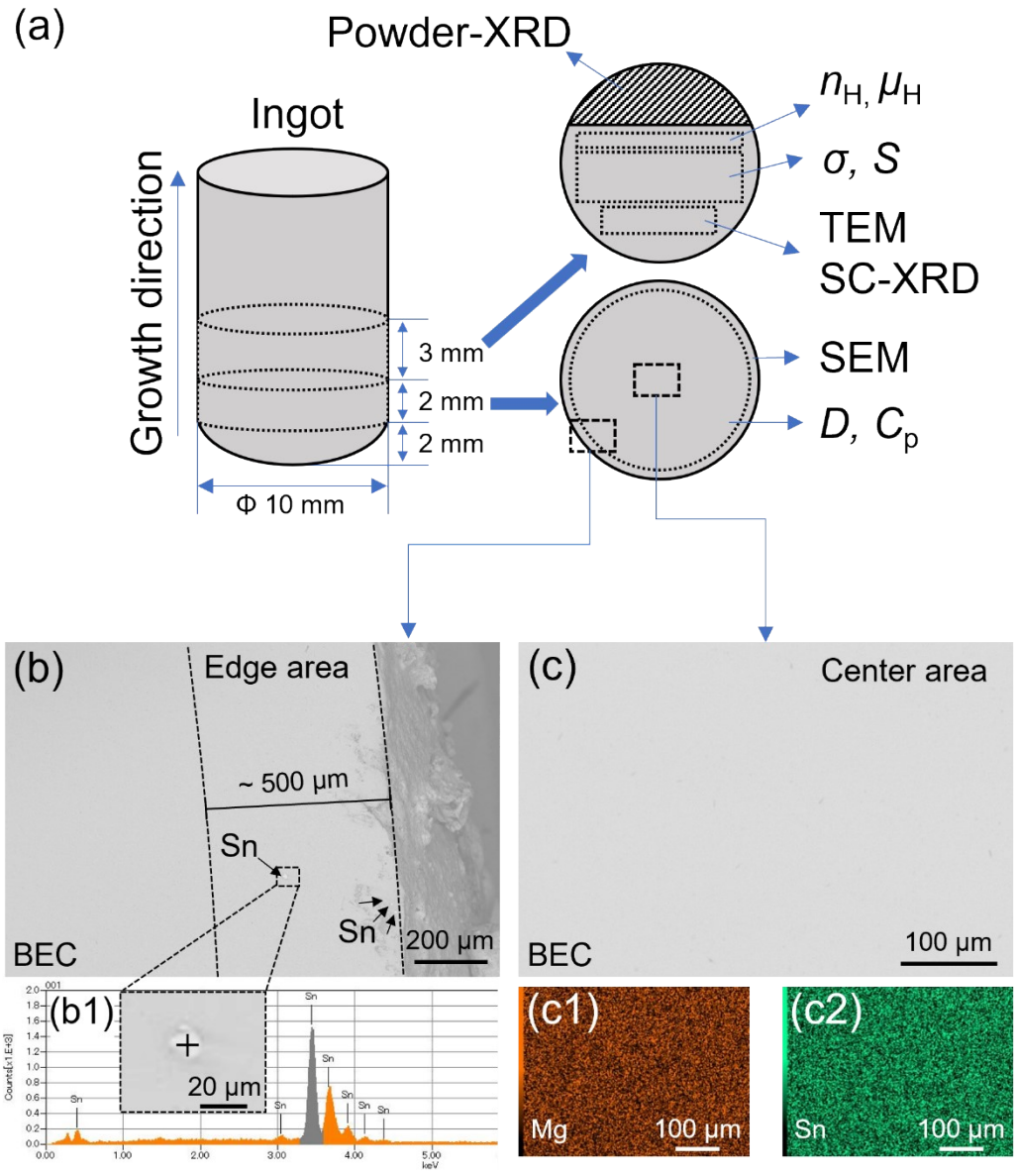

Figure S1. (a) Sample positions in the $Mg_{2-x}Li_xSn$ ingots used for each measurement. (b) SEM image at the edge of the x = 0.02 ingot. In (b1), the EDX analysis of a white dot is shown. (c) SEM image at the center of the x = 0.02 ingot. In (c1) and (c2), elemental mapping images of the same region of (c) are shown.

Laue X-ray diffraction (XRD)

Figures S2a-e show the Laue XRD patterns of the $Mg_{2-x}Li_xSn$ (x = 0,[1] 0.005, 0.015, 0.020, and 0.025) ingots. The patterns coincided with a simulation for the Mg_2Sn phase along the [111] direction (Figure S2f), indicating that the $Mg_{2-x}Li_xSn$ ingots were single crystals (SCs).

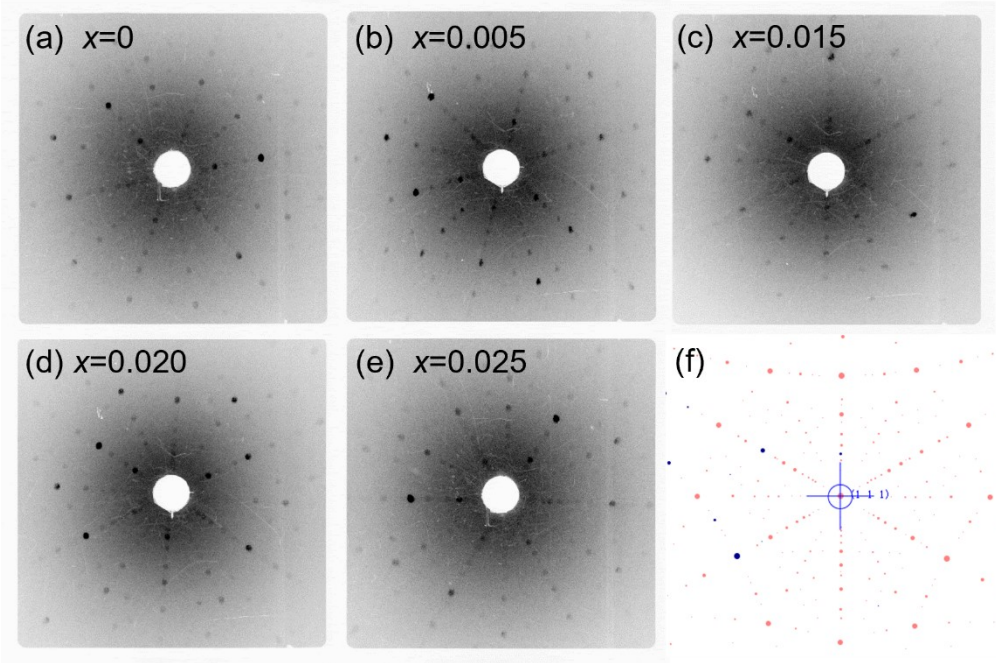

Figure S2. (a-e) Laue XRD patterns of the $Mg_{2-x}Li_xSn$ (x = 0,[1] 0.005, 0.015, 0.020, and 0.025) ingots. (f) Simulated Laue XRD pattern for the Mg_2Sn phase along the [111] direction.

SC-XRD

For the crystal structure analysis of the $Mg_{2-x}Li_xSn$ SCs, we performed SC-XRD. A structure model of $Mg_{2-x}Li_xSn$ with Mg vacancies (V_{Mg}) was used. Table S1 lists the evaluated $_wR$-factor, good-of-fitness (gof), Mg site occupancy, and equivalent isotropic displacement parameters U_{iso} of the $Mg_{2-x}Li_xSn$ (x = 0.005, 0.015, 0.020, and 0.025) SCs obtained from the SC-XRD. The V_{Mg} fraction was derived by subtracting the Mg/Li occupancy from 100%.

Table S1. $_wR$ factor, gof, and refined structural parameters for the $Mg_{2-x}Li_xSn$ (x = 0.005, 0.015, 0.020, and 0.025) SCs.

X	$_wR$ (%)	gof	Mg/Li occupancy at the Mg site (%)†	U_{iso} of Mg (Å^2)	U_{iso} of Sn (Å^2)
0.005	2.05	1.61	94.55(120)/0.25	0.0116(4)	0.00778(15)
0.015	2.98	2.38	89.45(200)/0.75	0.0100(7)	0.00744(15)
0.020	2.88	2.39	89.00(180)/1.00	0.0097(7)	0.00730(15)
0.025	4.04	3.08	84.50(300)/1.50	0.0089(11)	0.0066(2)

†The Li content was fixed to the nominal composition.

Transmission electron microscope (TEM) observation

Nanoscale precipitates around 44 nm (17 – 69 nm in size) were examined in a low-magnification TEM image of the $Mg_{1.980}Li_{0.020}Sn$ (x = 0.020) SC, as shown in Figure S3a. Figure S3b shows the electron diffraction pattern from the region containing several precipitates (the white dash circle in Figure S3a).

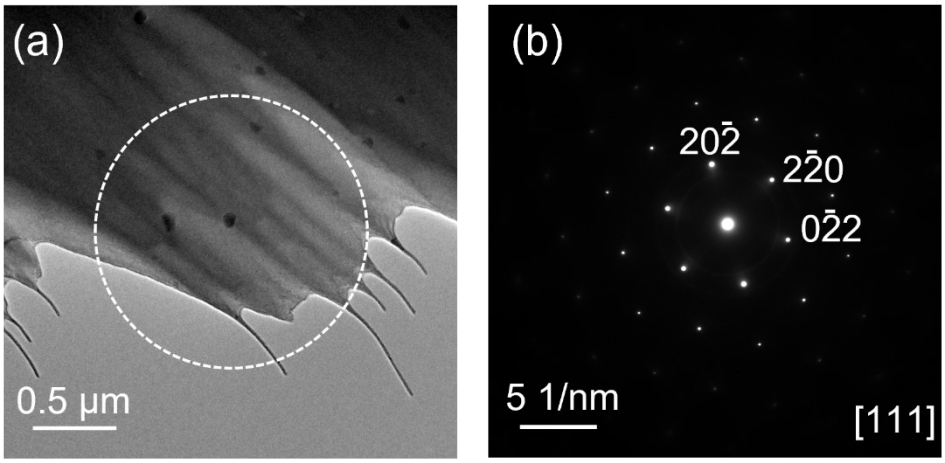

Figure S3. (a) Low-magnification TEM image of the $Mg_{1.980}Li_{0.020}Sn$ (x = 0.020) SC. (b) Electron diffraction pattern from the region inside the white dash circle of Figure S2a.

Electronic thermal conductivity

The electronic thermal conductivity, κ_{el}, was estimated using the Wiedemann-Franz law: $\kappa_{el} = L\sigma T$, where L, σ, and T are the Lorenz number, electrical conductivity, and absolute temperature, respectively. The L value was calculated from the measured Seebeck coefficient, S, using:[2]

$$L = 1.5 + exp\left(-\frac{|S|}{116}\right). \quad \text{(S1)}$$

The deviation of L is within 5%.[2] This is because the electronic band structure and a dominant phonon scattering mechanism of Mg_2Sn are a single parabolic band and acoustic phonon scattering, respectively.

Figure S4 shows the estimated κ_{el} of the $Mg_{2-x}Li_xSn$ (x = 0,[1] 0.005, 0.015, 0.020, and 0.025) SCs as a function of temperature. The κ_{el} increased with increasing the Li content x. By the Li-doping, κ_{el} became higher than the 2% Ga-doped Mg_2Sn SC,[1] reflecting the higher σ of the $Mg_{2-x}Li_xSn$ SCs.

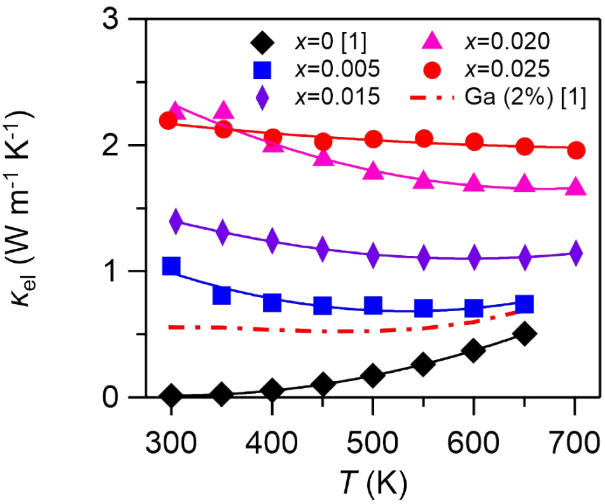

Figure S4. Temperature dependence of κ_{el} of the $Mg_{2-x}Li_xSn$ (x = 0.005, 0.015, 0.020, and 0.025) SCs. The data of the undoped and 2% Ga-doped Mg_2Sn SC[1] are also shown for comparison.

Bipolar thermal conductivity

The bipolar thermal conductivity κ_{bip} was given by the following equation:[3]

$$\kappa_{bip} = \frac{\sigma_e \sigma_h}{\sigma_e + \sigma_h}(S_e - S_h)^2 T, \quad \text{(S2)}$$

where σ_e, σ_h, S_e, and S_h are the electron conductivity, hole conductivity, electron Seebeck coefficient, and hole Seebeck coefficient, respectively. The σ_e, σ_h, S_e, and S_h were calculated by fitting the measured σ and S using the following equations:[3]

$$\sigma = \sigma_e + \sigma_h, \quad \text{(S3)}$$

$$\sigma_e = n_e e \mu_e, \quad \text{(S4)}$$

$$\sigma_h = n_h e(A\mu_e), \quad \text{(S5)}$$

$$n_e = 4\pi\left(\frac{2m_e^* k_B T}{h^2}\right)^{\frac{3}{2}} F_{\frac{1}{2}}(\xi), \quad \text{(S6)}$$

$$n_h = 4\pi\left(\frac{2m_h^* k_B T}{h^2}\right)^{\frac{3}{2}} F_{\frac{1}{2}}(-\xi - \xi_G), \quad \text{(S7)}$$

$$S = \frac{\sigma_e S_e + \sigma_h S_h}{\sigma}, \quad \text{(S8)}$$

$$S_e = -\frac{k_B}{e}\left[\frac{\left(r + \frac{5}{2}\right) \cdot F_{r+\frac{3}{2}}(\xi)}{\left(r + \frac{3}{2}\right) \cdot F_{r+\frac{1}{2}}(\xi)} - \xi\right], \quad \text{(S9)}$$

$$S_h = \frac{k_B}{e}\left[\frac{\left(r + \frac{5}{2}\right) \cdot F_{r+\frac{3}{2}}(-\xi - \xi_G)}{\left(r + \frac{3}{2}\right) \cdot F_{r+\frac{1}{2}}(-\xi - \xi_G)} + \xi + \xi_G\right], \quad \text{(S10)}$$

$$\xi_G = \frac{E_g - bT}{k_B T}, \quad \text{(S11)}$$

where n_e, n_h, e, μ_e, A, m_e^*, m_h^*, k_B, h, $F_n(\xi)$, ξ, ξ_G, r, E_g, and b are the electron carrier concentration, hole carrier concentration, elementary charge, fitting parameter, electron

effective mass, hole effective mass, Boltzmann constant, Plank constant, Fermi integral, reduced Fermi energy, temperature-dependent band gap, scattering parameter (here, r = -1/2), band gap, and temperature coefficient, respectively. The used parameters are presented in Table S2. The calculation details can be found in our previous papers.[4-6]

Table S2. Parameters used for the calculation of the κ_{bip} of the $Mg_{2-x}Li_xSn$ (x = 0.005, 0.015, 0.020, and 0.025) SCs.

	E_g (eV)	b (eV/K)	A	m_e^*	m_h^*
x = 0.005	0.36 [7]	3×10^{-4} [7]	1	1.08	0. 507
x = 0.015	0.36 [7]	3×10^{-4} [7]	1	1.08	0. 497
x = 0.02	0.36 [7]	3×10^{-4} [7]	1	1.08	0. 588
x = 0.025	0.36 [7]	3×10^{-4} [7]	1	1.08	0. 525

The temperature dependence of κ_{bip} of the $Mg_{2-x}Li_xSn$ SCs is shown in Figure S5. The calculated κ_{bip} of the undoped and 2% Ga-doped Mg_2Sn SCs[1] is also shown. The κ_{bip} decreased as the Li content x increased, confirming the suppression of bipolar conduction by increasing the majority carriers, i.e., hole carriers due to the Li-doping.

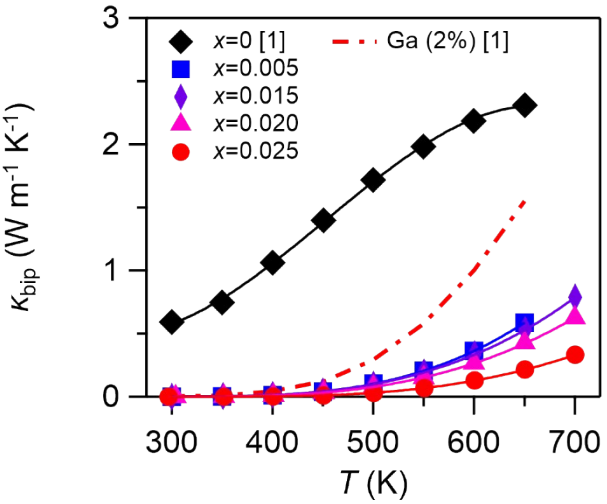

Figure S5. Temperature dependence of κ_{bip} of the $Mg_{2-x}Li_xSn$ (x = 0.005, 0.015, 0.020, and 0.025) SCs, with the undoped and 2% Ga-doped Mg_2Sn SCs.[1]

Lattice Thermal Conductivity

The lattice thermal conductivity, κ_{lat}, was calculated by using the Debye model:[8]

$$\kappa_{lat}(x) = \frac{k_B}{2\pi^2 v}\left(\frac{k_B T}{\hbar}\right)^3 \int_0^{\frac{\theta_D}{T}} \frac{x^4 e^x}{\tau_{tot}^{-1}\left(e^x - 1\right)^2} dx,\ x \equiv \frac{\hbar\omega}{k_B T}, \quad \text{(S12)}$$

where v, $\hbar$, θ_D, τ_{tot}, and ω are the sound velocity, reduced Planck constant, Debye temperature, total relaxation time for phonon scattering, and phonon frequency, respectively.

Considering that phonons are scattered by the Umklapp process (UP; three phonon scattering process), point defects (PDs), dislocation cores (DCs) and nano precipitates (NPs), the τ_{tot}^{-1} can be described by the following equation:[9]

$$\tau_{tot}^{-1}(\omega) = \tau_{UP}^{-1}(\omega) + \tau_{PD}^{-1}(\omega) + \tau_{DC}^{-1}(\omega) + \tau_{NP}^{-1}(\omega), \quad \text{(S13)}$$

The relaxation time of UP is given as:

$$\tau_{UP}^{-1}(\omega) = \frac{\hbar\gamma^2}{M v^2 \theta_D}\omega^2 T e^{\left(-\frac{\theta_D}{3T}\right)}, \quad \text{(S14)}$$

where the γ and M are the Grüneisen parameter and average atomic mass, respectively. The relaxation time of PD scattering is given by

$$\tau_{PD}^{-1}(\omega) = \frac{V_0 \omega^4}{4\pi v^3}\Gamma, \quad \text{(S15)}$$

where the V_0, and Γ are the average atomic volume and disorder parameter, respectively. The PD scattering mainly comes from two aspects: mass fluctuation and stain. Thus, the Γ can be described as following equations:[10,11]

$$\Gamma = \Gamma_{Mg} + \Gamma_{Sn}, \quad \text{(S16)}$$

$$\Gamma_{Mg} = \Gamma_{Mg(V_{Mg})} + \Gamma_{Mg(Li)}, \quad \text{(S17)}$$

$$\Gamma_{Mg(V_{Mg})} = \frac{2}{3}\left(\frac{\bar{M}_{Mg}}{\bar{M}}\right)^2 p(1-p-q)\left\{\left[\frac{M_{V_{Mg}} - M_{Mg}}{pM_{V_{Mg}} + (1-p-q)M_{Mg}}\right]^2 + \varepsilon_{Mg}\left[\frac{r_{V_{Mg}} - r_{Mg}}{pr_{V_{Mg}} + (1-p-q)r_{Mg}}\right]^2\right\}, \quad \text{(S18)}$$

$$\Gamma_{Mg(Li)} = \frac{2}{3}\left(\frac{\bar{M}_{Mg}}{\bar{M}}\right)^2 q(1-p-q)\left\{\left[\frac{M_{Li} - M_{Mg}}{qM_{Li} + (1-p-q)M_{Mg}}\right]^2 + \varepsilon_{Mg}\left[\frac{r_{Li} - r_{Mg}}{qr_{Li} + (1-p-q)r_{Mg}}\right]^2\right\}, \quad \text{(S19)}$$

$$\Gamma_{Sn} = 0, \quad \text{(5)}$$

where the average atomic mass is denoted as $\bar{M}$ (considering both the Mg and Sn sites)

and $\bar{M}_{Mg}$ (at the Mg site); p and q represent the V_{Mg} fraction and Li dopant content, respectively; M is the atomic mass and r is the atomic radius, with subscripts of V_{Mg}, Mg, Li ($M_{V_{Mg}}$= 0 u, $r_{V_{Mg}}$= 0 Å); ε_{Mg} is the strain field factor at the Mg site. The evaluated Γ_{Mg}, Γ_{Sn}, and Γ values are presented in Table S3. The relaxation time of the phonon scattering by the DCs, τ_{DC}^{-1} was calculated by:

$$\tau_{DC}^{-1}(\omega) = N_{DC}\frac{V^{4/3}\omega^3}{v^2}, \quad \text{(S20)}$$

where the N_{DC} is the density of the DCs. The expression to estimate the relaxation time of NPs, τ_{NP}^{-1}, is given by

$$\tau_{NP}^{-1}(\omega) = v\left[\left(2\pi R^2\right)^{-1} + \left(\pi R^2 \frac{4}{9}\left(\frac{\Delta\rho}{\rho_0}\right)^2\left(\frac{\omega R}{v}\right)^4\right)^{-1}\right]V_{NP}, \quad \text{(S21)}$$

where V_{NP} is the density of the NPs (here, $V_{NP} = 2.6\times10^{20}$ m^{-3}), R is the average radius (here, $R = 2.2\times10^{-8}$ m), ρ_0 is the density of the matrix, i.e., the single crystal region of the Mg_2Sn phase, and $\Delta\rho$ is the density difference between the NP and the Mg_2Sn phase. The used parameters for the calculation of $\tau_{UP}(\omega)$, $\tau_{PD}(\omega)$, $\tau_{DC}(\omega)$, and $\tau_{NP}(\omega)$ are presented in Table S4.

Table S3. Calculated $\Gamma_{Mg(V_{Mg})}$, $\Gamma_{Mg(Li)}$, Γ_{Sn}, and Γ values of the $Mg_{2-x}Li_xSn$ (x = 0.005, 0.015, 0.020, and 0.025) SCs.

Li content x	$\Gamma_{Mg(V_{Mg})}$	$\Gamma_{Mg(Li)}$	Γ_{Sn}	Γ
0.005	0.0579	0.000171	0	0.0581
0.015	0.107	0.000512	0	0.107
0.020	0.108	0.000681	0	0.109
0.025	0.149	0.000850	0	0.150

Table S4. Parameters used for the calculation of κ_{lat} of the $Mg_{2-x}Li_xSn$ (x = 0.005, 0.015, 0.020, and 0.025) SCs.

v (m/s)	θ_D (K)	γ	ε_{Mg}	ε_{Sn}
3000 [12]	240 [13]	1. 95 [5]	8 [14]	23 [14]

References

(1) Z. Huang, K. Hayashi, W. Saito, Y. Miyazaki, *ACS Appl. Energy Mater.*, 2021, **4** 13044–13050.

(2) H.-S. Kim, Z.M. Gibbs, Y. Tang, H. Wang, G.J. Snyder, *APL Mater.*, 2015, **3**, 041506.

(3) J.R. Drabble, H.J. Goldsmid, Transport processes in an intrinsic semiconductor. Thermal Conduction in Semiconductors, (Eds. J.R. Drabble, H.J. Goldsmid), *Pergamon press*, 1961.

(4) W. Saito, K. Hayashi, J. Dong, J.-F. Li, Y. Miyazaki, *Sci. Rep.*, 2020, **10**, 2020.

(5) W. Saito, K. Hayashi, Z. Huang, J. Dong, J.-F. Li, Y. Miyazaki, *ACS Appl. Mater. Interfaces*, 2020, **12**, 57888-57897.

(6) W. Saito, K. Hayashi, Z. Huang, K. Sugimoto, K. Ohoyama, N. Happo, M. Harada, K. Oikawa, Y. Inamura, K. Hayashi, T. Miyazaki, Y. Miyazaki, *ACS Appl. Energy Mater.*, 2021, **4**, 5123–5131.

(7) U. Winkler, *Helv. Phys. Acta.*, 1955, **28**, 633-666.

(8) J. Callaway, H.C. von Baeyer, *Phys. Rev.*, 1960, **120**, 1149-1154.

(9) G.A. Slack, S. Galginaitis, *Phys. Rev.*, 1964, **133**, A253–A268.

(10) B. Abeles, *Phys. Rev.*, 1963, **131**, 1906–1911.

(11) G.A. Slack, *Phys. Rev.*, 1962, **126**, 427–441.

(12) L.C. Davis, W.B. Whitten, G.C. Danielson, *J. Phys. Chem. Solids*, 1967, **28**, 439–447.

(13) F.J. Jelinek, W.D. Shickell, B.C. Gerstein, *J. Phys. Chem. Solids*, 1967, **28**, 267–270.

(14) J. Xin, Y. Zhang, H. Wu, T. Zhu, T. Fu, J. Shen, S.J. Pennycook, X. Zhao, *Small Methods*, 2019, **3**, 1900412.